

Article

Electromagnetic Regulation of Electrolyte Solution Heat Convection in Microchannels

Miaomiao Song¹, Xiaoting Chi², Yahui Wang² and Yu Ma^{3,*}

¹ No. 703 Research Institute of China Shipbuilding Industry Corporation, Harbin 150078, China; 18846448849@163.com

² School of Energy Science and Engineering, Harbin Institute of Technology, Harbin 150001, China; cxt@stu.hit.edu.cn (X.C.); wangyahui@hit.edu.cn (Y.W.)

³ Sino-French Institute of Nuclear Engineering and Technology, Sun Yat-sen University, Zhuhai 519082, China

* Correspondence: mayu9@mail.sysu.edu.cn; Tel.: +86-0756-366-8967

Received: 27 April 2018; Accepted: 24 May 2018; Published: 28 May 2018



Abstract: With the rapid development of microelectronics and micro-electromechanical system technology, the electronic components have become smaller and the performance has become higher. Under this condition, however, their energy consumption and heat production have also increased continuously, which poses a great challenge to heat dissipation. In this paper, electromagnetic driving technology is applied to drive the electrolyte solution flow within a microchannel to realize efficient heat convection with microchannel walls. By changing the magnitude and direction of electric–magnetic field, the regulation of heat convection performance is studied. The results show that the Nu number of microchannel increases as the Ha number and magnetic direction angle increases, while it decreases as the potential difference increases. According to the average index of the four factors, it was determined that the electrolyte solution had the best heat convection performance with $Ha = 0.05$, $Vb = 0.00006$, $Pe = 90$, and $\alpha = 90^\circ$. After that, sensitivity analysis of the Ha number, potential difference and magnetic direction angle was used to regulate the heat convection performance. This paper may provide some theoretical support for the design of microelectronics and micro-electromechanical systems.

Keywords: microchannel; convection heat convection; electrolyte solution; electromagnetic regulation

1. Introduction

In recent years, the development of microelectronics and micro-electromechanical systems has undergone much investigation, which has made the electronic components smaller and the performance higher [1]. Under this condition, however, their energy consumption and heat production have also increased continuously [2], which poses a great challenge to heat dissipation. During operation, electronics shows great sensitivity to temperature and excessive temperature will reduce their performance and reliability [3]. Therefore, we must find a reasonable and effective heat dissipation method to control the temperature of electronic devices for better stability and safety during operation. The purpose of developing an electronic component cooling technology is to miniaturize and integrate existing liquid cooling techniques, so that these can be applied to microchannels [4]. To this end, how to drive liquid flow stably in the microchannel without vibration and noise was the focus of the current research.

In order to achieve stable flow in microchannels and narrow microchannels, the flow characteristics and influencing factors need to be studied first. On this issue, many researchers have carried out a lot of valuable research, which provides strong support for later work [5–7]. After comparison, the application of magnetohydrodynamics (MHD) may be a good choice.

MHD is the phenomenon by which a conductive liquid undergoes a Lorentz force and moves under the action of mutually perpendicular magnetic and electric fields [8]. Recently, the application of MHD has played an important role in many engineering fields, including aerodynamics [9], metallurgy [10], thermonuclear experimental reactors [11], and others [12], owing to its attractive advantages [13], such as high flexibility, low application voltage, great economy, no moving parts, highly driving force, high safety and reliability. Some studies of its application in microfluidics have been made. Parashar et al. [14] and Krause et al. [15] introduced the application of MHD in electromechanical dynamics and liquid metal, respectively. They argued that the MHD effect should be considered in these phenomena. Zhang et al. [16] numerically studied the acceleration/deceleration control of three-dimensional MHD flow in a channel. After numerical simulation, the relationship between the acceleration/deceleration effect and electric–magnetic fields were determined. Jang et al. [17] studied a novel micropump, which pumping mechanism was based upon MHD principles, and the performance of the MHD micropump obtained theoretically in a single phase was compared with the experimental results. Ahmed et al. [18] numerically simulated a direct current (DC) electromagnetic pump for liquid aluminum at a large Reynolds number under an externally-imposed, non-uniform magnetic field. Lim et al. [19] presented a continuous flow MHD micropump with side walled electrodes using Lorentz force, and established a theoretically simplified MHD flow model. To study the combined influences of electro–magneto–hydrodynamic forces in controlling the fluid flow, Chakraborty et al. [20] developed a mathematical model for parallel plate rectangular microchannels. The results shows that the volumetric flow rates substantial increased with a low-magnitude magnetic field but stopped increasing with a high-magnitude magnetic field. Based on the above, the MHD-driven technique can be treated as a stable driving method. However, most of this work focused on the fluid flow in microchannels without considering heat convection. The study of heat convection in microchannels originated from the transport phenomena in porous media. Many works on this issue provide rich experience for the benefit of later research [21]. Yazdi et al. [22] studied MHD liquid flow and heat transfer over a non-linear permeable stretching surface in the presence of chemical reactions and partial slip. The analytical solution in this research may be potentially influential in controlling wall shear stress as well as the local Nusselt and Sherwood numbers. Sarkar et al. [23] analyzed the effect of nanofluids on thermally fully-developed MHD flows through microchannels.

Current studies of MHD-driven convection heat transfer in microchannels mainly focus on nanofluids and metal fluids, and research on the heat convection of electrolytes in microchannels has not yet been reported. To improve this situation, this paper proposes the use of electromagnetic drive to achieve the flow and heat convection of the electrolyte solution in the microchannel. Through dimensionless derivation, the standard parameters of the heat convection for the electrolyte solution under the electromagnetic drive are obtained. The flow of the electrolyte solution in the microchannel and its heat convection control method are studied by numerical simulation.

2. Physical Modeling

This section introduces the physical model of the electromagnetic-driven electrolyte solution in a three-dimensional rectangular microchannel, as shown in Figure 1. The length, height and width of the microchannel are denoted by L , H and W , respectively, and the temperature of the walls is denoted by T_w . The microchannel is filled with KCl electrolyte solution with initial temperature T_0 at the inlet, and $T_w > T_0$. Two electrodes with potential difference V_0 are applied to the left and right surfaces, resulting in a current density \mathbf{J} (x -direction). A magnetic field with strength \mathbf{B} is applied in z -direction. These two fields generate a Lorentz force $\mathbf{J} \times \mathbf{B}$, which drives the electrolyte solution to flow along the $+y$ direction of the microchannel and heat exchange with the surrounding walls.

Since the thickness of the double layer of the electrolyte solution in the channel (~10 nm) is much smaller than that of the microchannel, the ion distribution of the electrolyte solution can be assumed to be uniform. The electric field distribution can be described by the Poisson equation [1,24,25]:

$$\nabla^2 V = \nabla \cdot (\mathbf{u} \times \mathbf{B}), \tag{1}$$

$$E = -\nabla V, \tag{2}$$

where \mathbf{u} is the flow velocity, and V is the electric potential.

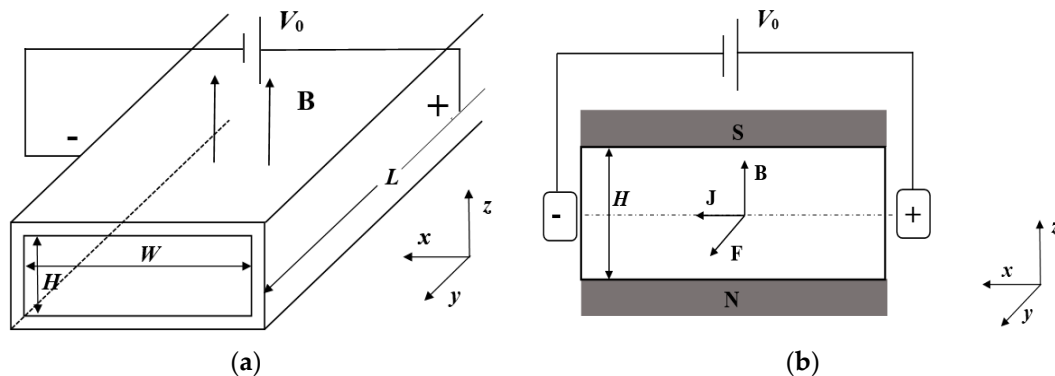


Figure 1. Schematic diagram of a rectangle electromagnetically-driven microchannel. (a) Three-dimensional model schematic; (b) Two-dimensional schematic diagram of x - z cross-section.

According to Ohm’s law, the current density can be expressed as [26]:

$$\mathbf{J} = \sigma(-\nabla V + \mathbf{u} \times \mathbf{B}), \tag{3}$$

where σ is the conductivity of the solution; and $\mathbf{u} \times \mathbf{B}$ represents the induced electromotive force generated by the ions moving in the electric field.

Due to the small geometry and magnetic Reynolds number, the induced magnetic field can be neglected, so that only the external magnetic field needs to be considered. Therefore, the flow process of the incompressible electrolyte solution under the Lorentz force can be described as the continuity and Navier–Stokes equations:

$$\nabla \cdot \mathbf{u} = 0, \tag{4}$$

$$-\nabla p + \mu \nabla^2 \mathbf{u} + \mathbf{J} \times \mathbf{B} = 0, \tag{5}$$

where \mathbf{u} is flow velocity; ρ and μ denote the density and viscosity of the fluid, and p denotes the pressure.

The energy conservation of the electrolyte solution under electromagnetic drive is described by

$$\rho C_p \mathbf{u} \cdot \nabla T = \lambda \nabla^2 T + \frac{\mathbf{J} \cdot \mathbf{J}}{\sigma}, \tag{6}$$

where T is the temperature of the fluid; C_p is the specific heat capacity; λ is the thermal conductivity of the electrolyte solution; $\mathbf{J} \cdot \mathbf{J} / \sigma$ represents the Joule heat source term [27].

To analyze the model mechanism and not be affected by the dimensions, non-dimensionalization is necessary. The dimensionless scaling parameters are defined as follows: dimensionless length:

$$x^* = \frac{x}{H}, \quad y^* = \frac{y}{H}, \quad z^* = \frac{z}{H}, \tag{7}$$

dimensionless magnetic induction strength:

$$\mathbf{B}^* = \frac{\mathbf{B}}{\mathbf{B}_0}, \tag{8}$$

dimensionless electric potential:

$$V^* = \frac{V}{V_0}, \tag{9}$$

dimensionless current density:

$$\mathbf{J}^* = \mathbf{J}/(\sigma V_0/W), \tag{10}$$

dimensionless speed:

$$\mathbf{u}^* = \frac{\mathbf{u}}{\mathbf{u}_0}, \tag{11}$$

dimensionless pressure:

$$p^* = \frac{p}{p_0}, \tag{12}$$

dimensionless time:

$$t^* = \frac{t}{t_0}, \tag{13}$$

dimensionless temperature:

$$T^* = \frac{T}{T_0}, \tag{14}$$

in which \mathbf{B}_0 is the maximal field strength; V_0 is the maximal potential applied to the electrolyte; and \mathbf{u}_0 , p_0 , t_0 , and T_0 are defined as follows:

$$\mathbf{u}_0 = \frac{\sigma V_0 \mathbf{B}_0 H^2}{\mu W}, \quad p_0 = \frac{\mu \mathbf{u}_0}{H}, \quad t_0 = \frac{H}{\mathbf{u}_0}, \quad T_0 = \frac{(\sigma V_0/W)^2 H}{\sigma \rho C_p}. \tag{15}$$

Through non-dimensionalization, Equations (1), (3), (5) and (6) can be rewritten as:

$$\nabla^{*2} V^* = \frac{\mathbf{u}_0 \mathbf{B}_0 H}{V_0} \nabla^* \cdot (\mathbf{u}^* \times \mathbf{B}^*), \tag{16}$$

$$\mathbf{J}^* = -\zeta \nabla^* V^* + Ha^2 \mathbf{u}^* \times \mathbf{B}^*, \tag{17}$$

$$-\nabla^* p^* + \nabla^{*2} \mathbf{u}^* + \mathbf{J}^* \times \mathbf{B}^* = 0, \tag{18}$$

$$\mathbf{u}^* \cdot \nabla^* T^* = \frac{1}{Pe} \nabla^{*2} T^* + \frac{\mathbf{J}^* \cdot \mathbf{J}^*}{\sigma}, \tag{19}$$

where $\zeta = H/W$ is the aspect ratio of the microchannel; $Pe = \rho C_p \mathbf{u}_0 H/\lambda$ is the Berkeley number, which characterizes the relative strength of convection and diffusion; $Ha = \mathbf{B}_0 H \sqrt{\sigma/\mu}$ is the Hartmann number that characterizes the ratio of electromagnetic force and viscous force; and $Vb = \frac{\mathbf{u}_0 \mathbf{B}_0 H}{V_0}$ is defined as the characteristic number of the electric field, characterizing the ratio of the electromagnetic force and the electric field force.

3. Results and Discussion

3.1. Model Validation

To verify the present numerical model, an infinitely long rectangular microchannel [26] is tested. When the electric and magnetic fields are applied to the four walls, respectively, satisfying $H \ll W \ll L$, as shown in Figure 1, the velocity of the fully developed flow is isothermally expressed as:

$$\mathbf{u}_x(z) = -Ha^{-2} \left(\zeta \frac{dV}{dy} + \frac{dp}{dx} \right) \left[1 - \frac{\cosh(Haz)}{\cosh\left(\frac{Ha}{2}\right)} \right], \tag{20}$$

in which $\frac{dV}{dy} = -E = const$ denotes the electric field intensity in the y -direction.

In order to verify the reliability of this model, the velocity distribution of three-dimensional isothermal fully developed flow for the electrolyte solution is calculated firstly under the electromagnetic driving condition.

The KCl electrolyte solution with a concentration of 100 mM is adopted as the working liquid with $\sigma = 10 \text{ (m}\Omega\text{)}^{-1}$, $\mu = 0.001 \text{ Pa}\cdot\text{s}$, $\mathbf{B} = 0.4 \text{ T}$ and $H = 100 \text{ }\mu\text{m}$. Figure 2 shows the numerical solutions of the velocity distributions along the middle section ($W/2$), which are compared with the analytical solutions obtained from Equation (20).

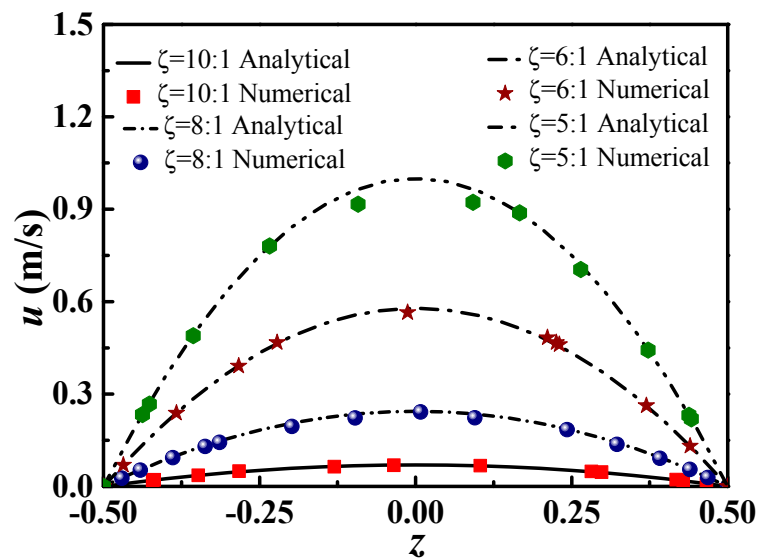


Figure 2. The speed of the middle section along z-direction at different aspect ratios.

As shown in Figure 2, the numerical solutions agree well with the analytical solutions with a large aspect ratio, indicating that the proposed model is accurate and reliable. In considering the small aspect ratio, the numerical solutions are slightly different from the analytical solutions, indicating that the analytical model cannot accurately describe the flow process in the electromagnetically-driven microchannel, and strict three-dimensional numerical simulation methods should be adopted.

3.2. Microchannel Heat Convection

3.2.1. Temperature Distribution in the Microchannel

Figures 3 and 4 show the temperature distribution in the microchannel under the electromagnetically-driven system, with boundary temperature $T_w = 323.15 \text{ K}$ and initial temperature $T_0 = 293.15 \text{ K}$. The aspect ratio of the microchannel is 2. The electrolyte solution flows through the microchannel to achieve heat convection, and its temperature significantly increases at the outlet. Figure 4 shows the temperature distribution along the midline of the x - z plane at a different y -direction position. As shown in Figure 4, as the fluid flow and the temperature distribution of the electrolyte solution becomes flat, and the temperature near the high-potential wall is obviously higher than that of low-potential wall. Therefore, it can be concluded that the heat convective of the electromagnetically-driven electrolyte solution is better on the high-potential wall than low-potential wall. Since the induced electromotive force generated by fluid flow introduces a stronger velocity near the high-potential wall, the heat convection is more intense, and the temperature of the electrolyte solution near the high-potential wall increase significantly.

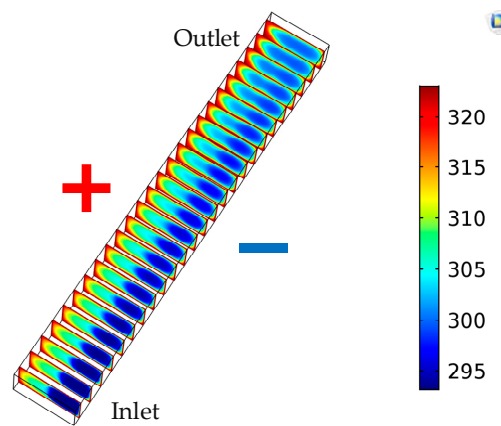


Figure 3. Temperature distribution of various x - z planes along the y -direction.

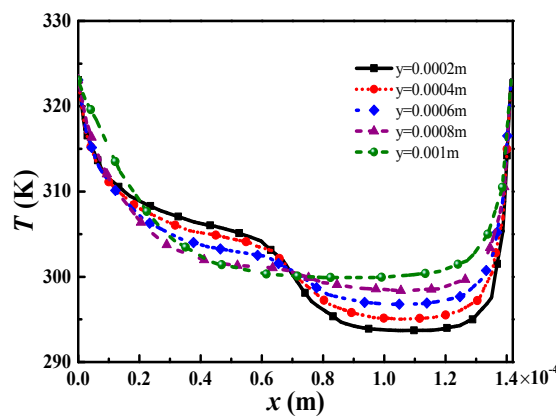


Figure 4. Temperature distribution on the midline of different cross sections along the y -direction.

3.2.2. Influence of Magnetic Strength on Microchannel Heat Convection

The Nu number and Ha number represent the heat convection ability and the magnetic strength, respectively. To study their relationship, the Nu number of the electromagnetically-driven electrolyte solution was calculated at different Ha numbers, in which the sodium chloride solution was adopted as the coolant. The inlet temperature was set to 293.15 K, and the microchannel wall temperatures were set to 323.15 K, and were constant during the whole simulation.

Figure 5 demonstrates an increase in the Nu number with an increase in the Ha number regardless of the shape or aspect ratio. The latter increase results in increases in the electromagnetic driving force and the consequent flow speed of the solution, enhancing the heat convection characterized by the Nu number. For a certain Ha number, the Nu number increases as the aspect ratio decreases. Equation (18) shows that the current density increases as the aspect ratio decreases, thus a larger Lorentz force will be produced to enhance heat convection. Figure 5 also shows that the heat convection of the circular microchannel was more intensive than that of square microchannel. This is because in the case of the same cross-section perimeter, the area of the circular cross-section is larger than that of the rectangular cross-section, which led to more electrolytic solution flows and stronger heat convection.

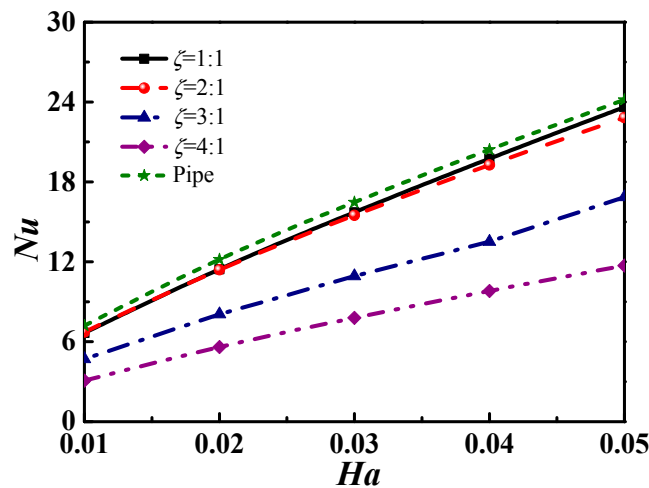


Figure 5. The Nu number varies with Ha number in microchannels with different cross-sectional shapes.

3.2.3. Influence of Magnetic Direction on Microchannel Heat Convection

For certain microchannels and magnetic fields, an effective way to change the Nu number is to reset the angular direction of the magnetic field. To this end, in this part, the influence of the magnetic direction on the Nu number will be analyzed and discussed.

As shown in Figure 6, the angle α between the magnetic field and the axis of the microchannel is defined as the magnetic direction angle. The Lorentz force applied to the charged ions changes along with changes in the direction angle α .

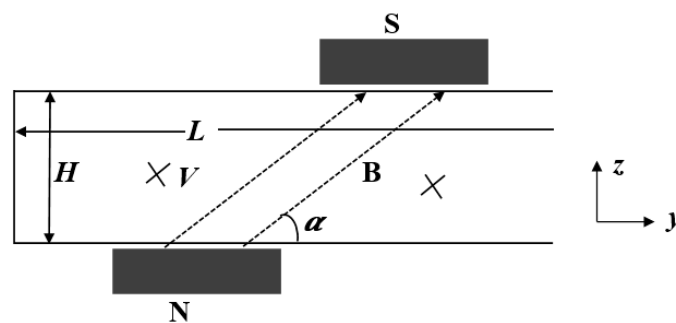


Figure 6. Two-dimensional cross-section of a microchannel that changes the magnetic field angle.

Under this condition, the momentum equation is modified as [28]:

$$\frac{\partial \rho u_y}{\partial t} + \nabla \cdot (\rho \mathbf{u} u_y) = -\frac{\partial p}{\partial y} + \nabla \cdot (\mu \nabla \cdot u_y) + F_y, \tag{21}$$

$$\frac{\partial \rho u_z}{\partial t} + \nabla \cdot (\rho \mathbf{u} u_z) = -\frac{\partial p}{\partial z} + \nabla \cdot (\mu \nabla \cdot u_z) + F_z, \tag{22}$$

in which \mathbf{u} satisfies $\mathbf{u} = j \cdot u_y + k \cdot u_z$; and F_y and F_z represent the magnetic field volume forces along y - and z -directions, which can be expressed as:

$$F_y = \sigma u_y |B \sin \alpha|^2, \tag{23}$$

$$F_z = \sigma u_z |B \cos \alpha|^2, \tag{24}$$

Figure 7 shows the changes in the Nu number along with angle α increasing with different Ha numbers. The aspect ratio of the square microchannel was set to 3:1. The figure shows that the Nu number increases as the angle α increases. The Nu number reaches its maximum at $\alpha = 90^\circ$, since under this direction the induced Lorentz force is parallel to the microchannel axis, and the velocity of the solution reaches the maximum [26].

Figure 7 demonstrates that an increase in Ha number will enhance the regulation effect of the magnetic direction. The Lorentz force is more significantly affected by the angle α with a large Ha number. Besides, when

the angle α is $60^\circ \sim 80^\circ$, the Nu number varies most obviously due to the significant change of the sine value and the volumetric force.

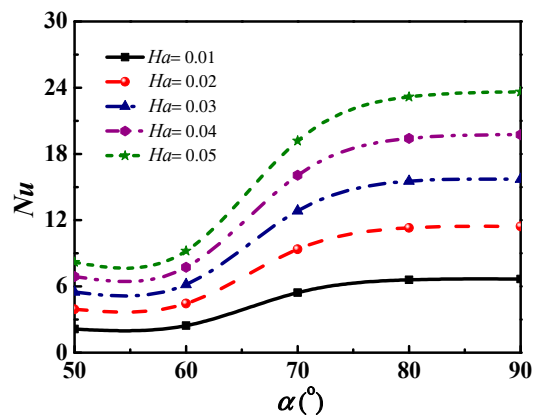


Figure 7. The Nu number varies with the magnetic direction in microchannels with an aspect ratio 3:1.

3.2.4. Influence of Potential on Microchannel Heat Convection

For a certain microchannel, the heat convection can be regulated by adjusting the potential difference between two electrodes. Figure 8 shows that the Nu number decreases as the Vb increases, due to the inverse proportion between the Vb number and the potential difference. Therefore, the increase in Vb will reduce the potential difference and the Lorentz force of the ion.

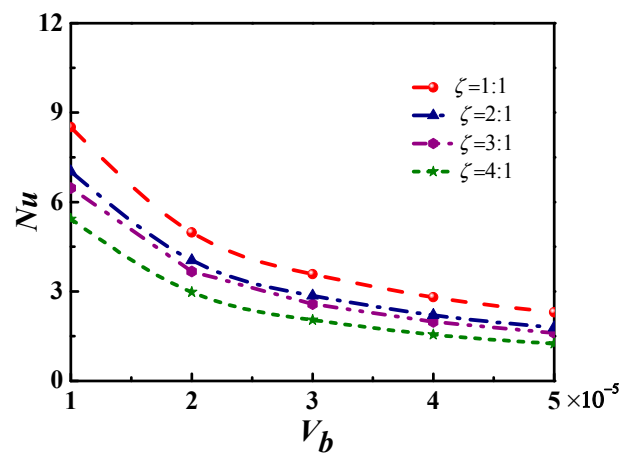


Figure 8. The Nu number changes with the Vb in the microchannel with different cross-sections, while the wall temperature is 323.15 K.

3.3. Impact Degree Analysis by the Orthogonal Experimental Method

3.3.1. Design of the Orthogonal Experiment

As can be seen from the previous discussion, the heat convection performance of the electromagnetically-driven electrolyte solution microchannel will be mainly influenced by the Ha number, Vb number, angle α , and Pe number. In this part, a set of orthogonal experiments is designed to analyze the impact degree of these four factors. Five levels were selected for each factor, as shown in Table 1.

Table 1. Parameter table of four factors with five levels.

No	A <i>Ha</i>	B <i>Vb</i>	C <i>Pe</i>	D α/o
1	0.01	0.00005	50	50
2	0.02	0.00006	60	60
3	0.03	0.00007	70	70
4	0.04	0.00008	80	80
5	0.05	0.00009	90	90

Using the orthogonal experimental method, 25 groups of calculation parameters were established to compare the impact degree of the four factors. The results for the *Nu* number are listed in Table 2, and their influences on heat convection were determined based on the numerical results. The data is discussed in the following section.

Table 2. Orthogonal design table and results for the four factors with five levels.

No	A <i>Ha</i>	B <i>Vb</i>	C <i>Pe</i>	D α/o	<i>Nu</i>
1	0.01	0.00005	50	50	1.06572
2	0.01	0.00006	60	60	1.23486
3	0.01	0.00007	70	70	2.94283
4	0.01	0.00008	80	80	3.64544
5	0.01	0.00009	90	90	3.67242
6	0.02	0.00005	60	70	10.48453
7	0.02	0.00006	70	80	12.36321
8	0.02	0.00007	80	90	11.29287
9	0.02	0.00008	90	50	4.20961
10	0.02	0.00009	50	60	2.6126
11	0.03	0.00005	70	90	27.48634
12	0.03	0.00006	80	50	9.16169
13	0.03	0.00007	90	60	10.00211
14	0.03	0.00008	50	70	11.859
15	0.03	0.00009	60	80	15.03036
16	0.04	0.00005	80	60	8.98464
17	0.04	0.00006	90	70	38.16797
18	0.04	0.00007	50	80	24.98374
19	0.04	0.00008	60	90	26.42209
20	0.04	0.00009	70	50	9.42444
21	0.05	0.00005	90	80	78.24366
22	0.05	0.00006	50	90	42.04679
23	0.05	0.00007	60	50	14.3471
24	0.05	0.00008	70	60	16.38925
25	0.05	0.00009	80	70	35.78468

3.3.2. Range Analysis

The average values and range analyses for the orthogonal experimental results for the 25 groups are shown in Table 3, in which the average values of the four influencing factors including *A* (*Ha* number), *B* (*Vb* number), *C* (*Pe* number), and *D* (angle α) are calculated. A_5 , B_2 , C_5 , and D_5 are the priority levels of the four factors, respectively. The order of these elements according to the results is $A > D > B > C$. The range of *A* is the largest, indicating that the *Ha* number has the greatest effect on the heat convection. According to the index average value of these four factors, one can find that the best possible combination is A_5 - B_2 - C_5 - D_5 , namely the electrolyte solution in the microchannel. The best heat convection performance exists when $Ha = 0.05$, $Vb = 0.00006$, $Pe = 90$ and $\alpha = 90^\circ$ is satisfied.

Table 3. Index average and range analysis table of heat convection performance in the microchannel.

Factors	A	B	C	D
K_1	12.56127	57.44563	65.17455	38.20856
K_2	41.99269	102.97452	67.51894	45.26918
K_3	73.53946	64.59852	68.60603	99.23901
K_4	107.98288	62.52539	70.73961	134.2664
K_5	186.81148	66.5245	84.29577	136.95034
\bar{K}_1	2.512254	11.489126	13.03491	7.641712
\bar{K}_2	8.398538	20.594904	13.503788	9.053836
\bar{K}_3	14.707892	12.919704	13.721206	19.847802
\bar{K}_4	21.596576	12.505078	14.147922	26.853282
\bar{K}_5	37.362296	13.3049	16.859154	27.390068
Priority level	A_5	B_2	C_5	D_5
R_i	34.850042	9.105778	3.824244	19.748356
Sequence	$A > D > B > C$			

3.4. Sensitivity Analysis of Microchannel Heat Convection Performance

To quantitatively regulate the heat convection of the microchannel, a sensitivity analysis was made for the Ha number, Vb number and angle α .

The sensitivity coefficient is defined as the ratio of the relative rate of change of the objective function to that of the uncertain influence factors, whose expression is written as follows [28]:

$$E = \frac{\Delta A/A}{\Delta F/F} \tag{25}$$

where A denotes the objective function, F denotes the uncertain influence factor, and E denotes the sensitivity coefficient of the objective function A to the uncertain influence factor F . The larger E becomes, the greater the sensitivity coefficient corresponding to the uncertain influence factor.

3.4.1. Sensitivity Analysis of Ha Number

Firstly, the sensitivity of the Ha number on the Nu number was analyzed when the magnetic direction was perpendicular to the axis of the microchannel; the results are shown in Figure 9.

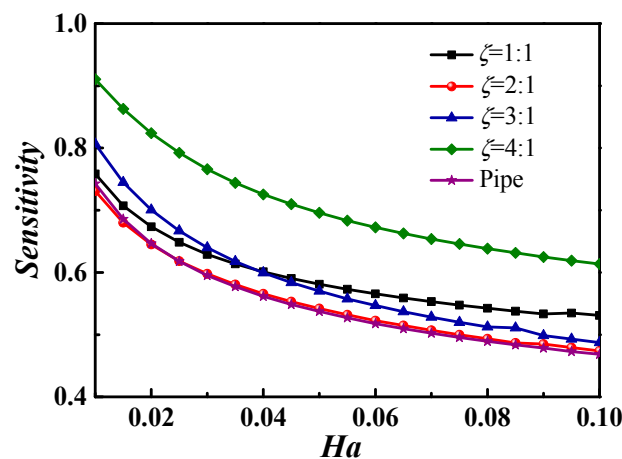


Figure 9. Sensitivity of the Ha number to the Nu number with various cross-sections.

Figure 9 illustrates decreases in both the sensitivity coefficient of the Nu and the decline rate of the sensitivity with an increase in the Ha , when the Ha ranges from 0.01 to 0.1, indicating a stronger regulating ability of the Ha at a smaller Ha number. Figure 9 also shows that the sensitivity of the aspect ratio 4:1 was obviously larger than that of the other square microchannels, and the sensitivity of the circle microchannel (denoted by pipe) was the lowest.

3.4.2. Sensitivity Analysis of Vb

This part studies the sensitivity of the Vb number on the Nu number. Figure 10 demonstrates that the sensitivity of the Vb number is negative, since the Vb number is inversely proportional to the potential difference. The sensitivity decreases as the Vb number increases, meaning that the regulating ability of the Vb number on Nu is stronger at a smaller Vb number, and weaker at a larger Vb number. The sensitivity coefficients with different aspect ratios show that the aspect ratio has a small impact on the sensitivity coefficient. The sensitivity of the aspect ratio 1:1 and 4:1 was slightly larger than that of other microchannels.

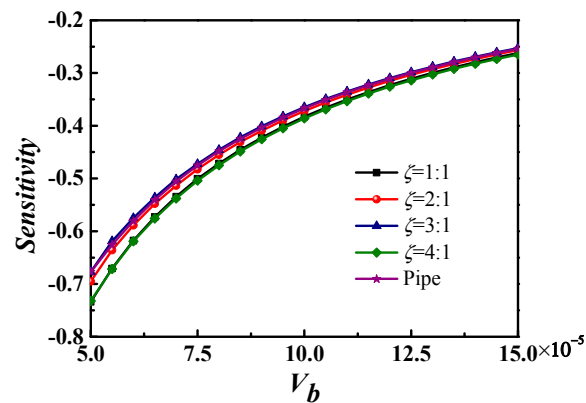


Figure 10. Sensitivity of the Vb number to the Nu number with various cross-sections.

3.4.3. Sensitivity Analysis of the Magnetic Direction

At last, the sensitivity of the magnetic direction angle α on the Nu number is analyzed; the results are shown in Figure 11. When the angle α varies from 60° to 90° , the sensitivity coefficient of the Nu number increases obviously as the angle α increases, and reaches maximum at $\alpha = 70^\circ$. After that, the sensitivity coefficient decreases slowly. Therefore, the magnetic direction angle has the strongest adjustment ability to the Nu number at about 70° , and the larger direction angle (over 70°) has a stronger adjustment ability than smaller angles (below 70°). The sensitivity coefficient of different aspect ratios shows that the regulating ability of the magnetic direction on the Nu number with an aspect ratio of 4:1 is obviously better than that of other aspect ratios.

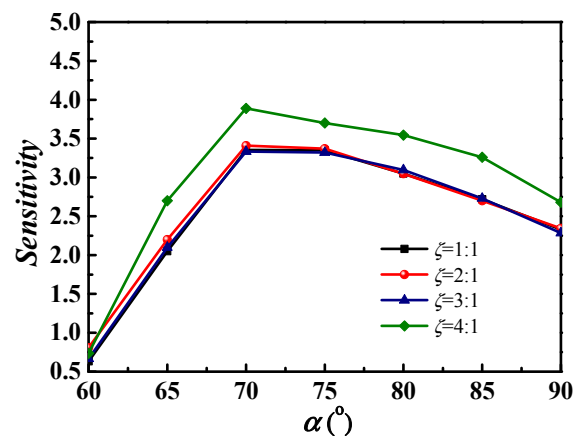


Figure 11. Sensitivity coefficient of magnetic direction on the Nu number with various cross-sections.

4. Conclusions

The development of microelectronics and micro-electromechanical system technology has produced a great challenge in terms of heat dissipation. To improve this situation, this paper systematically studied the heat convection of microchannels cooled by an electromagnetic driving electrolyte solution. By applying the electric and magnetic fields, the charged ions were driven by Lorentz force along the microchannel, so that efficient heat

convection within the microchannel is achieved. For a certain microchannel, the performance of heat convection can be regulated by changing the strength and direction of the magnetic field. The potential difference between electrodes also can provide effective regulation. After the numerical simulation of a microchannel, the following conclusions were drawn:

1. The heat convection of an electromagnetically-driving electrolyte solution microchannel is mainly influenced by the dimensionless characteristic parameters of Ha and Vb numbers. The Nu number increases as the Ha number and magnetic direction angle increases, and decreases as the Vb number increases.
2. After orthogonal experiments and range analysis, the degree of influence of the main factors of the heat convection in the microchannel is determined as follows: the Ha number, the magnetic direction angle, the Vb number, and the Pe number.
3. After sensitivity analysis, the regulation abilities of the main factors on the heat convection of the microchannel are determined. The first factor is the Ha number, which, if it is small enough, has a regulating ability on large Nu numbers. Similarly, the Vb number shows a strong regulating ability when the Vb number is small enough. The magnetic field has the strongest regulating ability when its direction angle is around 70° .

Author Contributions: Y. Ma provided the idea; Y. Ma and M. Song conceived and designed the project; Y. Wang, M. Song and X. Chi performed the simulation; Y. Ma, Y. Wang and M. Song validated and analyzed the data; X. Chi investigated the simulation; M. Song and Y. Ma drafted the manuscript; Y. Wang and X. Chi reviewed and modified the manuscript.

Acknowledgments: This work is supported by the State Key Program of National Natural Science of China under Grant No. 51436009.

Conflicts of Interest: The authors declare no conflict of interest.

References

1. Ando, T.; Ueno, K.; Taniguchi, S.; Takagi, T. Induction pump for high-temperature molten metals using rotating twisted magnetic field: Thrust measurement experiment with solid conductors. *IEEE Trans. Magn.* **2002**, *38*, 1789–1796. [[CrossRef](#)]
2. Marcinichen, J.B.; d'Entremont, B.P.; Thome, J.R. Thermal management of ultra intense hot spots with two-phase multi-microchannels and embedded thermoelectric cooling. In Proceedings of the ASME 2013 International Technical Conference and Exhibition on Packaging and Integration of Electronic and Photonic Microsystems. American Society of Mechanical Engineers, Burlingame, CA, USA, 16–18 July 2013; p. V001T04A023.
3. Kabbani, H.; Wang, A.H.; Luo, X.B.; Qian, S.Z. Modeling redox-based magnetohydrodynamics in three-dimensional microfluidic devices. *Phys. Fluids* **2007**, *19*, 083604. [[CrossRef](#)]
4. Qian, S.Z.; Bau, H.H. Magnetohydrodynamic stirrer for stationary and moving fluids. *Sens. Actuators B Chem.* **2005**, *106*, 859–870. [[CrossRef](#)]
5. Xiao, B.Q.; Zhang, X.; Wang, W.; Long, G.; Chen, H.; Kang, H.; Ren, W. A fractal model for water flow through unsaturated porous rocks. *Fractals* **2018**, *26*, 1840015. [[CrossRef](#)]
6. Long, G.B.; Xu, G.S. The effects of perforation erosion on practical hydraulic-fracturing applications. *SPE J.* **2017**, *22*. [[CrossRef](#)]
7. Xiao, B.Q.; Chen, H.X.; Xiao, S.X.; Cai, J.C. Research on relative permeability of nanofibers with capillary pressure effect by means of fractal-Monte Carlo technique. *J. Nanosci. Nanotechnol.* **2017**, *17*, 6811–6817. [[CrossRef](#)]
8. Qian, S.Z.; Zhu, J.Z.; Bau, H.H. A stirrer for magnetohydrodynamically controlled minute fluidic network. *Phys. Fluids* **2002**, *14*, 3584–3592. [[CrossRef](#)]
9. Gupta, A.K.; Beer, J.M.; Louis, J.F.; Busnaina, A.A.; Lilley, D.G. Flow aerodynamics modeling of an MHD swirl combustor—Calculations and experimental verification. *J. Fluid Eng.* **1982**, *104*, 179–189. [[CrossRef](#)]
10. Lemoff, A.V.; Lee, A.P. An AC magnetohydrodynamic micropump. *Sens. Actuators B Chem.* **2000**, *63*, 178–185. [[CrossRef](#)]
11. Hogan, J.T.; Martynov, A. Sensitivity of ITER MHD global stability to edge pressure gradients. *Fusion Sci. Technol.* **1994**, *26*, 322–326. [[CrossRef](#)]
12. Suh, Y.K.; Kang, S. A review on mixing in microfluidics. *Micromachines* **2010**, *1*, 82–111. [[CrossRef](#)]

13. Ho, J.E. Characteristic study of MHD pump with channel in rectangular ducts. *J. Mar. Sci. Technol.* **2007**, *15*, 315–321.
14. Woodson, H.H.; Melcher, J.R. *Electromechanical Dynamics*; John Wiley: Hoboken, NJ, USA, 2001.
15. Davidson, P.A. *An Introduction to Magnetohydrodynamics*; Cambridge University Press: Cambridge, UK, 2001.
16. Zhang, K.P.; Tian, Z.Y.; Feng, D.H.; Li, H. Numerical study of acceleration/deceleration control of three-dimensional magnetohydrodynamic flow in channel. *Acta Aerodyn. Sin.* **2009**, *27*, 258–268.
17. Jang, J.; Lee, S.S. Theoretical and experimental study of MHD (magnetohydrodynamic) micropump. *Sens. Actuators A Phys.* **2000**, *80*, 84–89. [[CrossRef](#)]
18. Ahmed, D.; Nedeltcho, K. Magneto-hydrodynamic numerical study of DC electromagnetic pump for liquid metal. In Proceedings of the COMSOL Conference, Hannover, Germany, 4–6 November 2008; pp. 133–146.
19. Lim, S.; Choi, B. A study on the MHD (magnetohydrodynamic) micropump with side-walled electrodes. *J. Mech. Sci. Technol.* **2009**, *23*, 739–749. [[CrossRef](#)]
20. Chakraborty, S.; Paul, D. Microchannel flow control through a combined electromagnetohydrodynamic transport. *J. Phys. D Appl. Phys.* **2006**, *39*, 5364–5371. [[CrossRef](#)]
21. Xiao, B.Q.; Wang, W.; Fan, J.T.; Chen, H.; Hu, X.; Zhao, D.; Zhang, X.; Ren, W. Optimization of the fractal-like architecture of porous fibrous materials related to permeability, diffusivity and thermal conductivity. *Fractals* **2017**, *25*, 1750030. [[CrossRef](#)]
22. Yazdi, M.H.; Abdullah, S.; Hashim, I.; Sopian, K. Slip MHD liquid flow and heat convection over non-linear permeable stretching surface with chemical reaction. *Int. J. Heat Mass Trans.* **2011**, *54*, 3214–3225. [[CrossRef](#)]
23. Sarkar, S.; Ganguly, S. Fully developed thermal transport in combined pressure and electroosmotically driven flow of nanofluid in a microchannel under the effect of a magnetic field. *Microfluid Nanofluid* **2015**, *18*, 623–636. [[CrossRef](#)]
24. Outhwaite, C.W.; Bhuiyan, L.B. An improved modified Poisson–Boltzmann equation in electric-double-layer theory. *J. Chem. Soc. Faraday Trans.* **1983**, *79*, 707–718. [[CrossRef](#)]
25. Ramos, J.I.; Winowich, N.S. Finite difference and finite element methods for MHD channel flows. *Int. J. Numer. Methods Fluids* **1990**, *11*, 907–934. [[CrossRef](#)]
26. Qian, S.Z.; Bau, H.H. Magneto-hydrodynamics based microfluidics. *Mech. Res. Commun.* **2009**, *36*, 10–21. [[CrossRef](#)] [[PubMed](#)]
27. Vaibhav, P.; Samuel, K.K. Electroosmosis and thermal effects in magnetohydrodynamic (MHD) micropumps using 3D MHD equations. *Sens. Actuators B Chem.* **2007**, *122*, 42–52.
28. Song, D.X.; Jing, D.W.; Luo, B. Modeling of anisotropic flow and thermodynamic properties of magnetic nanofluids induced by external magnetic field with varied imposing directions. *J. Appl. Phys.* **2015**, *118*, 8971–8979. [[CrossRef](#)]

